Extended Data Figures.

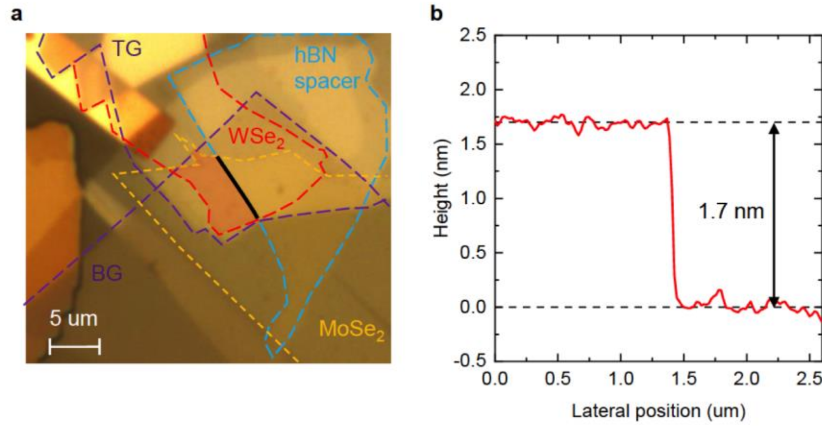

Extended Data Figure 1 | Device image. a, Optical image of the $MoSe_2/WSe_2$ device presented in the main text (Device 1). The dashed lines mark the boundaries of the top and bottom graphite gates (purple), the $MoSe_2$ monolayer (yellow), the WSe_2 monolayer (red), and the thick hBN spacer in the contact region (light-blue). The thin hBN spacer that separates the two TMD layers is not shown. The black solid line marks the boundary of the contact region and the region of interest (shaded). **b,** Atomic force microscopy (AFM) profile of the thin BN spacer, showing a step height of ∼1.7 nm (~ 6-layer).

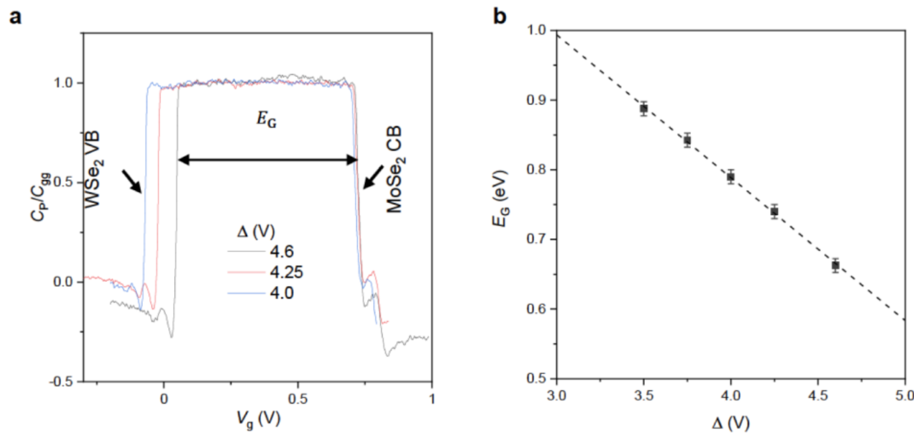

Extended Data Figure 2 | Dependence of interlayer band gap on anti-symmetric gating. a, Gate dependence of penetration capacitance at 15 K under varying anti-symmetric gating Δ and $V_b = 0$ V. The step falls signify electron doping into the $MoSe_2$ conduction band (CB) or hole doping into the WSe_2 valence band (VB). The separation between the rising and falling edges determines the band gap E_G. An additional step on the electron-doping side arises from the presence of a small non-overlapped $MoSe_2$ monolayer inside the dual-gated device that affects the penetration capacitance. **b,** Interlayer band gap E_G (symbols) extracted from **a** as a function of Δ. The linear fit (dashed line) has a slope of ~ $0.21e$. The gap energy extrapolated for Δ = 0 corresponds to the intrinsic band gap energy $E_G^0 \approx 1.6$ eV.

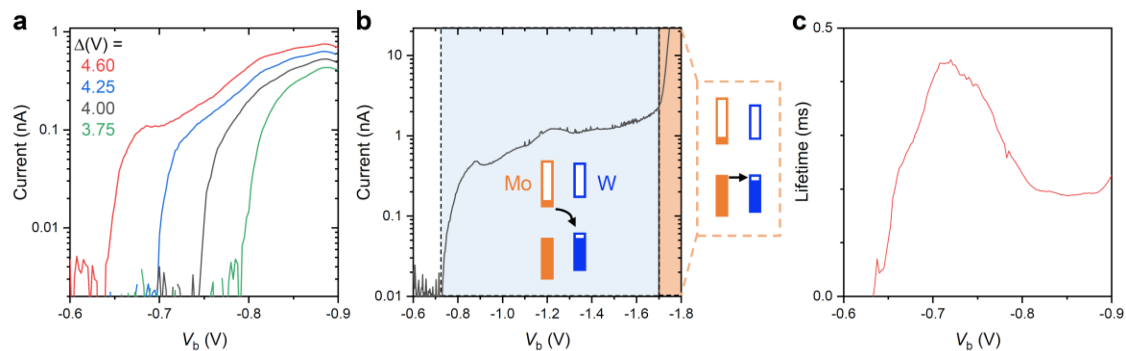

Extended Data Figure 3 | Tunneling current and exciton lifetime. a, Bias-dependent interlayer tunneling current of device 1 under $\Delta = 4.6$ V (red), 4.25 V (blue), 4.00 V (black), and 3.75 V (green). The shift of the onset with Δ is caused by the changing interlayer band gap. **b,** Interlayer tunneling current over a larger bias range at $\Delta = 4$ V. The insets illustrate both the non-resonant (blue-shaded) and resonant (orange-shaded) tunneling regimes. **c,** Estimated exciton lifetime as a function of V_b from the tunneling data at $\Delta = 4.6$ V in **a**.

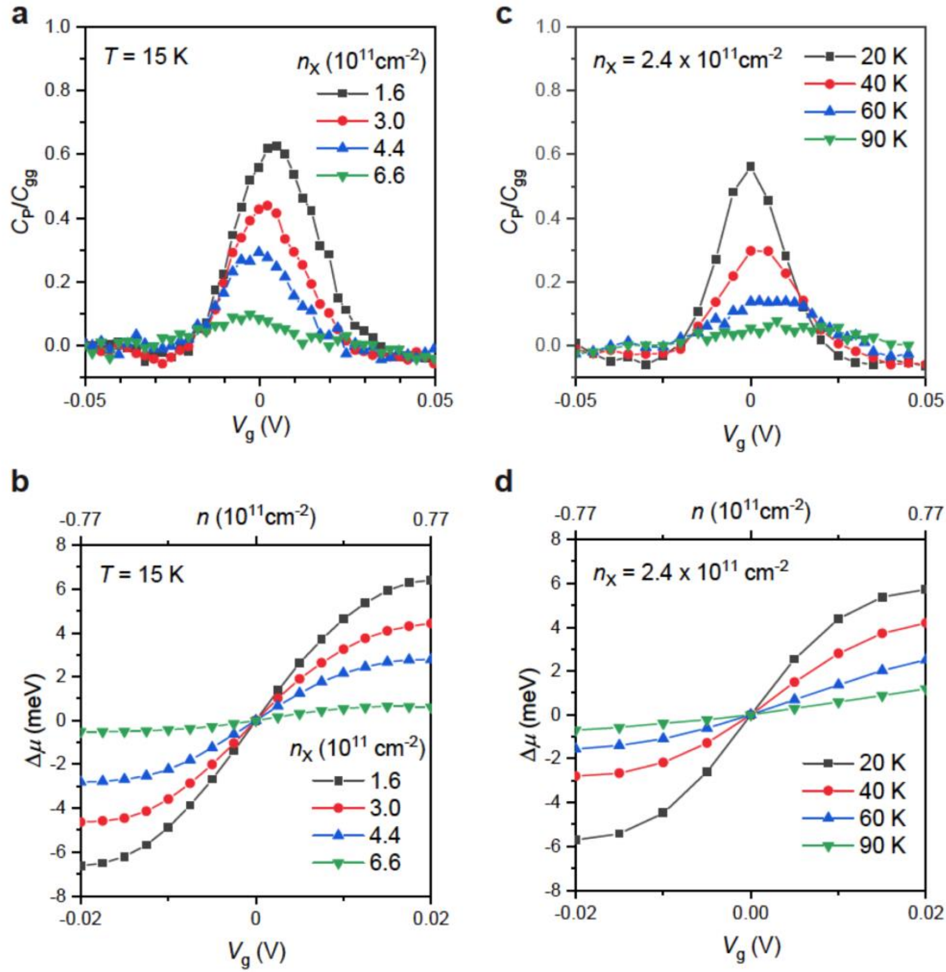

Extended Data Figure 4 | Determination of the charge gap. The penetration capacitance (**a**) and the charge chemical potential of the double layer (**b**) at 15 K as a function of V_g at varying exciton densities. The capacitance peak shows the presence of a charge-incompressible state. The integrated area of the peak gives the chemical potential jump (or the charge gap) at equal electron-hole density. The zero point of the chemical potential shift in **b** has been shifted to $V_g = 0$ V for comparison of different exciton densities. The charge gap closes near the Mott density. **c, d,** Similar to **a, b,** at a fixed exciton density $n_X = 2.4 \times 10^{11}$ cm^{-2} for different temperatures. The charge gap closes at the ionization temperature.

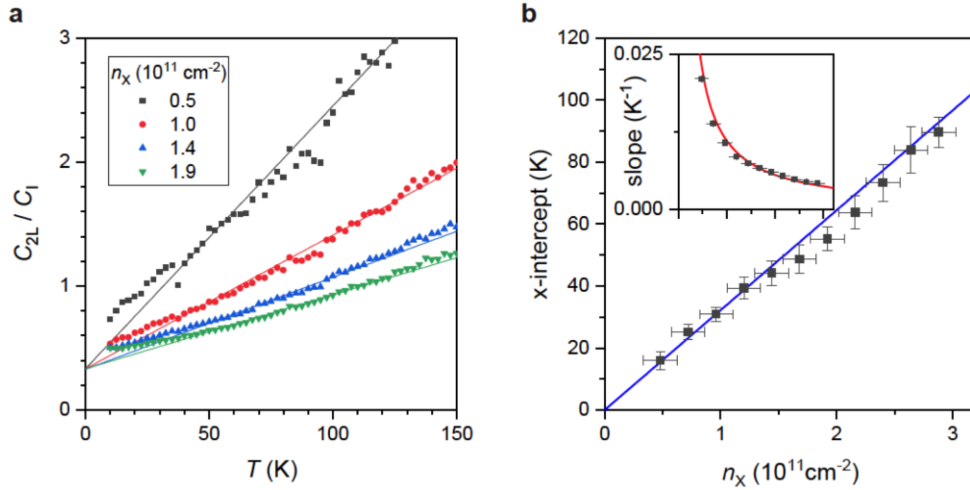

Extended Data Figure 5 | Exciton compressibility in the high-temperature limit. a, Inverse interlayer capacitance (or exciton compressibility) as a function of temperature at varying exciton densities. The lines are linear fits in the high-temperature limit, i.e. $gn_X/k_B \lesssim T \lesssim T_s$. **b,** Amplitude of the extracted x-intercept in **a** as a function of exciton density. A linear fit (blue) gives $g = (2.6 \pm 0.1) \times 10^{-14}$ eVcm^2. The inset shows the density dependence of the slope extracted from **a** (symbols). The red line is the mean-field result described in the main text. The density range is the same as in the main panel.

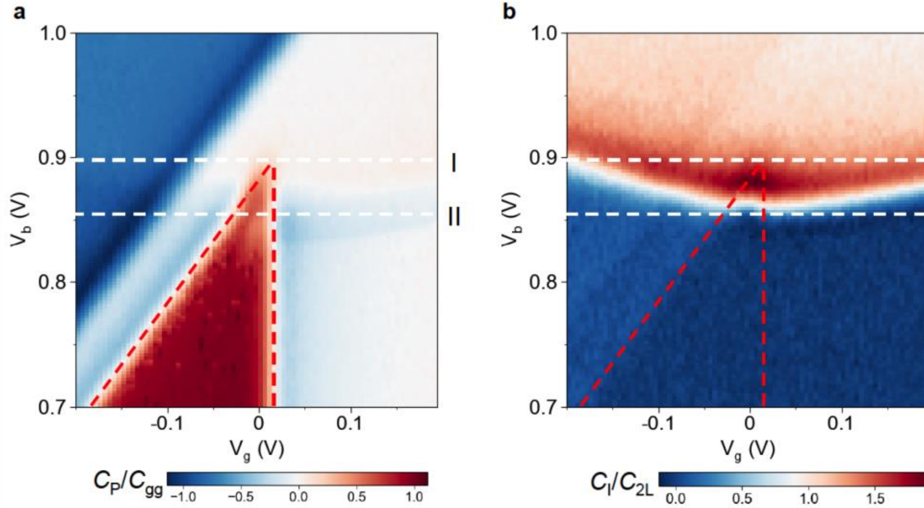

Extended Data Figure 6 | Main results from device 2. Penetration capacitance **(a)** and interlayer capacitance **(b)** as a function of bias and gate voltages. The Mo-layer is grounded. The two red dashed lines denote the conduction band edge of $MoSe_2$ (vertical line) and the valance band edge of WSe_2 (line with slope +1). The two white dashed lines denote the bias voltage at which the charge gap closes (I) and the exciton fluid becomes compressible (II). The difference between the two values (~ 40 mV) corresponds to the exciton binding energy at $n_X = 0$, which is slightly larger than in Device 1 shown in the main text (~ 25 mV) because the hBN barrier is slightly thinner (~ 5-layer).

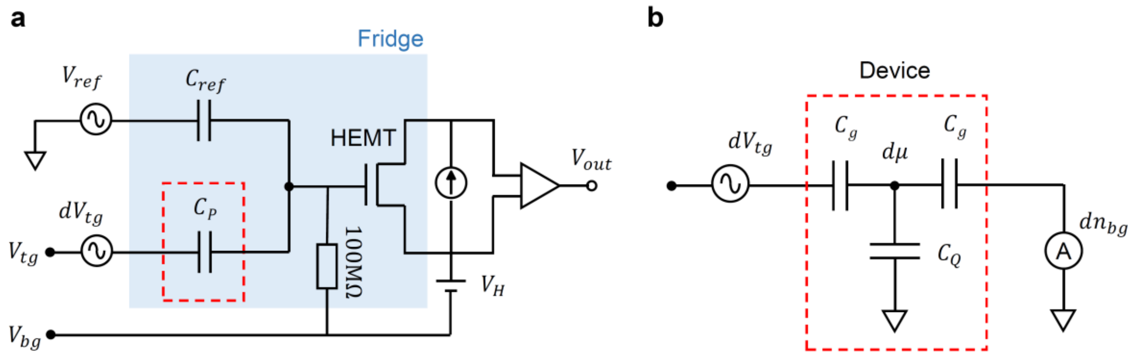

Extended Data Figure 7 | Circuit diagram. a, Circuit diagram for the penetration capacitance measurement. The red dashed line encloses the sample area. The reference part (V_{ref} and C_{ref}) is used to cancel the parasitic background capacitance. The HEMT is biased at voltage V_H. **b,** Equivalent circuit model of C_P in **a**. Here $C_g \approx 2C_{gg}$ is the sample-to-gate geometrical capacitance, which is about twice the gate-to-gate geometrical capacitance C_{gg}.

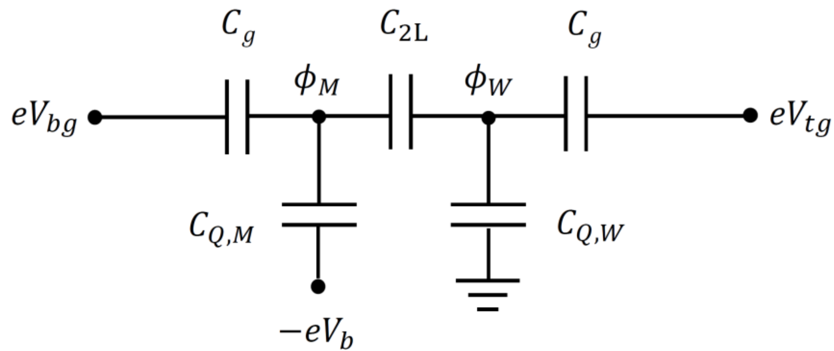

Extended Data Figure 8 | Equivalent device circuit model for electrostatics simulation. $C_{Q,M}$ and $C_{Q,W}$ are the quantum capacitances of the $MoSe_2$ and WSe_2 monolayers, respectively. Details see Methods.